Flood forecasting within urban drainage systems using NARX neural network

Yves Abou Rjeily, Oras Abbas, Marwan Sadek, Isam Shahrour and Fadi Hage Chehade

ABSTRACT

Urbanization activity and climate change increase the runoff volumes, and consequently the surcharge of the urban drainage systems (UDS). In addition, age and structural failures of these utilities limit their capacities, and thus generate hydraulic operation shortages, leading to flooding events. The large increase in floods within urban areas requires rapid actions from the UDS operators. The proactivity in taking the appropriate actions is a key element in applying efficient management and flood mitigation. Therefore, this work focuses on developing a flooding forecast system (FFS), able to alert in advance the UDS managers for possible flooding. For a forecasted storm event, a quick estimation of the water depth variation within critical manholes allows a reliable evaluation of the flood risk. The Nonlinear Auto Regressive with eXogenous inputs (NARX) neural network was chosen to develop the FFS as due to its calculation nature it is capable of relating water depth variation in manholes to rainfall intensities. The campus of the University of Lille is used as an experimental site to test and evaluate the FFS proposed in this paper.

Key words | case study, flooding forecast, NARX neural network, proactivity, urban drainage systems

Yves Abou Rjeily (corresponding author)
Oras Abbas
Marwan Sadek
Isam Shahrour
Lille University of Science and Technology,
Laboratoire de Génie Civil et Géo-Environnement,
Villeneuve d'Ascq,
France
E-mail: *yves.abourjeily@hotmail.com*

Yves Abou Rjeily
Marwan Sadek
Fadi Hage Chehade
Lebanese University,
Modeling Center,
Beirut,
Lebanon

INTRODUCTION

The fast growth of cities and the aging of their infrastructures are the main reasons behind the overstressing of urban drainage systems (UDS). Cities' expansion, not being accompanied by suitable drainage infrastructure upgrades, results in generating frequent flooding events, environment degradation and decreasing of groundwater recharge (Konrad & Booth 2002; Wang *et al.* 2003; Brandes *et al.* 2005). Furthermore, climate change affects rainfall intensity and patterns, and consequently the runoff volumes (Ponce *et al.* 1997; May 2008). This is leading to shortages in the capacity of the UDS (Berggren *et al.* 2012), and hence is causing frequent flooding appearances. The floods are difficult to predict and result in significant damage, economic consequences and casualties (Kenyon *et al.* 2008). Therefore, flood risks have become a major challenge for cities and a major concern for researchers and practitioners.

The first step in mitigating flooding impacts consists of understanding the actual system operation during the flooding events. Implementing a monitoring system combined with a hydraulic simulation model has proved efficient in analysing the UDS operation and flooding origins (Abou Rjeily *et al.* 2016). In recent years, dynamic management has shown a huge potential in increasing the capacities of these infrastructures, by optimizing their operations (Beeneken *et al.* 2013; Rocha *et al.* 2013; García *et al.* 2015). The efficiency of the dynamic management is highly dependent on the proactivity of the system managers and operators, which could be significantly enhanced by a flooding forecast system (FFS). An FFS consists of a model capable of predicting flooding occurrence and warning in advance the managers of the system.

Offering sufficient lead time to system operators to take preventive measures and apply optimal management strategies, an FFS is considered as an essential tool in mitigating flooding impacts. It is important to note that the complexity and dynamicity of UDS operations, together with temporal and spatial loading variability (Ocampo-Martinez 2010), make the construction of the FFS a demanding task, taking into consideration the time delays, constraints and nonlinearities. Traditionally, flooding forecasts are based on historical data and mathematical models or graphs that concern pattern recognition (Rajendra Acharya *et al.* 2003). Recently, black box models are used to allow the prediction of urban

doi: 10.2166/wst.2017.409

flooding occurrences. In order to accomplish this prediction, the models are trained on historical data and combined with rainfall radar forecasts (Duncan *et al.* 2013). FFSs developed using black box models have been applied largely for river analysis and protection, and have shown a good efficiency and practicality (Elsafi 2014; Perera & Lahat 2015; Amarnath *et al.* 2016; Artinyan *et al.* 2016), while for UDS, such systems are less developed and evaluated (Yen-Ming *et al.* 2010). Forecasting flooding in UDS is still based on deterministic simulation model results that require a lot of calculation time, which limits the efficiency and proactivity of the operators in taking the appropriate actions. With this in mind, this work focuses on developing a new methodology for implementing a feasible FFS for UDS.

METHODS

Proposed FFS

In this study, the proposed FFS will be focusing on quickly predicting the water depth variation in some critical locations of an UDS, instead of simulating the entire network operations. In order to achieve that, the engineers should first evaluate their system hydraulic capacity and analyse the flooding origins by conducting hydraulic simulations. Based on the simulation results, the locations of critical areas and manholes that should be monitored can be defined. The water depth variations within the defined critical manholes will be predicted through a black box model using forecasted rainfall intensities. The calculation engine of the FFS will be a black box model as described in the next paragraphs. The strategy steps for the FFS are as follows. Once the weather forecast detects the presence of rainfall events within the forecasted period, the black box model predicts the water depth variations at the critical locations of the UDS. If a forecasted water depth in any critical location exceeds a threshold defined by the engineers, the FFS alerts the managers of possible flooding. In response to the alert, infrastructure managers evaluate the severity of the situation, identify areas likely to be inundated and take appropriate actions and precautions. Actions and precautions could be as follows: informing specialist operators, warning inhabitants of underground basements, changing road signs for car drivers, etc.

The response of the UDS is a complex nonlinear function of the temporal and spatial variability of rainfall intensities. As mentioned earlier in this work, this complex function will be replaced by a black box model, trained to predict the water depth variation in some manholes according to the rainfall intensities. The use of a black box model, instead of conducting hydrologic–hydraulic simulation for the entire UDS operation, allows a significant reduction in the calculation time, which improves the proactivity of the operators. The water depth variation within a manhole, which represents the output of the complex function, depends on the rainfall intensity time series and the hydrologic modifications that occur during a storm event. The decrease in soil infiltration and in depression storage potential are examples of the hydrologic modifications that occur during a storm event.

NARX neural network for forecasting flooding events

The black box model, which will represent the calculation engine of the FFS in this study, should be able to account for rainfall intensity time series and to consider the hydrologic modifications occurring on the catchment. The NARX (Nonlinear Auto Regressive with eXogenous inputs) neural network combines exogenous input with recurrent behaviour in order to calculate its output. The exogenous input of the NARX neural network can represent the rainfall intensity time series. In addition, through its recurrent behaviour, a NARX neural network is able to differentiate the time factor within a storm event. Differentiating the time and understanding what was already happening in the UDS could enable the NARX neural network to account for the hydrologic modifications occurring during a storm event. Therefore, the NARX neural network and its calculation nature will be tested in the following sections, to evaluate its capacity to operate as the calculation engine for the proposed FFS.

Due to its efficiency in representing nonlinear dynamic behaviours (Hoffmeister 1991), the NARX model has been largely used in time series modelling and forecasting applications. The NARX model, presented in Equation (1), is characterized by calculating an output at the actual time step, as a function of multiple precedent inputs and outputs of the previous time steps.

$$y(t) = f[u(t-1),\ \ldots,\ u(t-n_u), y(t-1),\ \ldots, y(t-n_y)] \qquad (1)$$

where $y(t)$: model output time series, $u(t)$: model input time series, n_u and n_y: time delays required by the model in order to effectively represent the dynamic behaviour of the studied phenomenon.

NARX neural networks are highly efficient in simulating complex systems (Marsalek 2000). They have been used in different application types, as predictor for the next values of a time series and nonlinear noise filtering of input signals (Demuth *et al.* 2008). Their applicability has been proved in

multiple domains, including modelling gas turbines (Asgari *et al.* 2016), automated engineering (Tijani *et al.* 2014), wastewater treatment work (Çoruh *et al.* 2014), and environmental pollution (Hoffmeister 1991).

Two types of NARX neural network architecture were proposed in the literature (Menezes & Barreto 2008). The first type is series-parallel architecture, where the network uses the real precedent target values, which are measured values and the system tries to match $[y_{meas.}(t-1), \ldots, y_{meas.}(t-n_y)]$, with the input sequence $[u(t-1), \ldots, u(t-n_u)]$ in calculating the output at the next time step $[y(t)]$. Such architecture is efficient in forecasting a time series value for one time step ahead. The second type is the parallel architecture, which is based on using the sequence of the values calculated in previous time steps of the neural network $[y(t-1), \ldots, y(t-n_y)]$, instead of the real measured target values $[y_{meas.}(t-1), \ldots, y_{meas.}(t-n_y)]$, in calculating the output for the next time step $[y(t)]$. The parallel architecture of this network is used for predicting the output values for multiple time steps ahead. Since the FFS developed in this work is based on evaluating the water depth variation within some defined manholes for the total weather forecast period, the parallel architecture will be used in this study.

NARX neural network efficiency depends on the adopted structure and training process. The number of hidden layers and nodes, with time delays for exogenous inputs and recurrent outputs, constitutes the system structure. This structure is to be defined through iterative work. The training process of a neural network aims to find the most suitable weights of the neurons inter-connection channels and the bias values, which result in the best fit of the output data to the target values. Learning and training a neural network is a data-driven mechanism conducted on multiple iterations. After each iteration, the network updates the weights and bias values to get output values $[y(t)]$ closer to target values $[y_{meas.}(t)]$. Therefore, the training success is related to the size and quality of available historical data.

The methodology for implementing the FFS and the efficiency of the NARX neural network were tested on the stormwater network of the campus of the University of Lille.

APPLICATION AND RESULTS

Description of the site

The Lille University campus was used in order to develop and evaluate the proposed FFS, based on the NARX neural network. The university campus represents a small town of about 25,000 users, located in Villeneuve d'Ascq in northern France. Since 1960, the campus has been continuously expanded by the construction of new buildings and utilities. Water evacuation of the campus is conducted in two separated systems. This work concerns the stormwater network, presented in Figure 1. A sector of 30 ha was chosen on the campus for the development of the FFS, as shown in Figure 2. The UDS on this sector is composed of 8.44 km of pipelines with diameters ranging between 150 and 1,200 mm. This sector was chosen due to its vulnerability to flood, which occurs two to three times a year. Flooding zones are appearing near university buildings, including underground laboratories. The chosen sector contains, in addition to the pipes and manholes, some ancillary equipment including a lifting station, a check valve, a flow regulator and a retention tank.

Monitoring system implementation

In order to analyse the system hydraulic operation and understand the origins of the flood appearances, a monitoring system was implemented in March 2015 on the studied sector, as presented in Figure 3.

The monitoring system is composed of a weather station (a) for measuring the weather parameters such as rainfall intensities, temperature, and wind. The UDS was equipped with two depth meters for measuring the filling ratio of the existing retention tank (b), and the water depth variation at the last manhole of the studied sector (c). In addition, two flow meters were implemented within the underground pipes of the UDS, for measuring the flows generated from the entire studied sector (d), as well as a part of this sector (e). The monitoring system conducts measurements at a 1-minute time step, and sends data every hour to the database through a GPRS (general packet radio service) system. After cleaning and verifying the received data, through comparing the measurements to thresholds and to measurements of other sensors, collected data are used for evaluating the system operation at the implemented locations as well as calibrating a hydrologic–hydraulic simulation model.

Numerical modelling of the UDS hydraulic operation

In addition to the monitoring system implementation, a hydrologic–hydraulic simulation model of the UDS was constructed using the EPA-SWMM software, in order to extend the monitoring zones and to cover the entire system area. Auto-calibration of the EPA-SWMM model was accomplished through a hybrid optimization technique composed

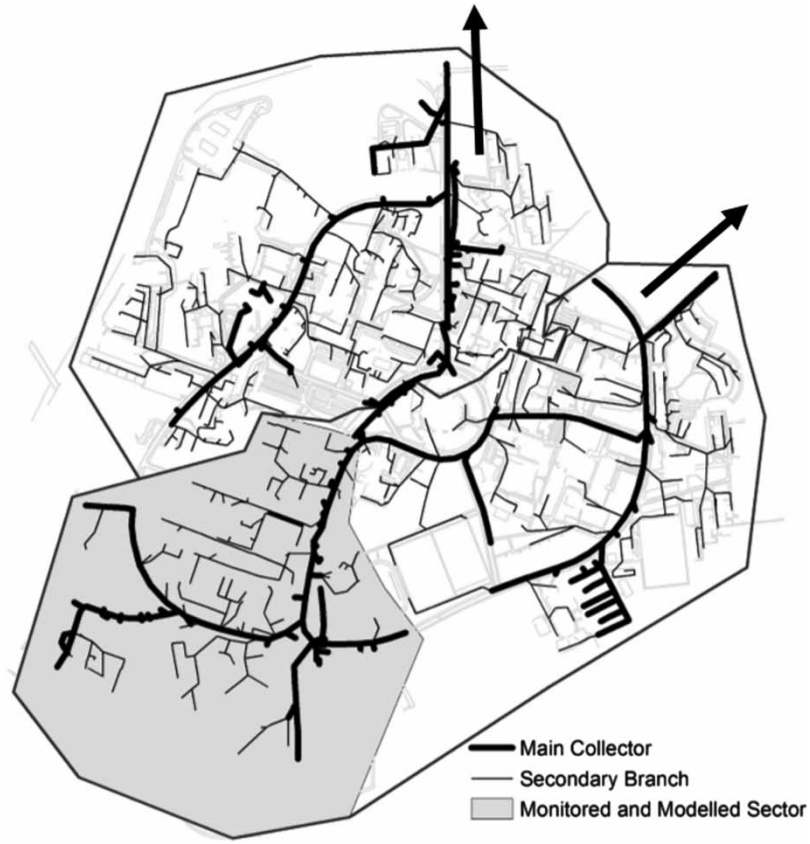

Figure 1 | Stormwater system of Lille University campus.

of a genetic algorithm followed by pattern search. The efficiency of the model calibration was examined through results and measurements comparison and Nash–Sutcliffe efficiency (NSE) calculation (Nash & Sutcliffe 1970). An NSE value of 1 represents a perfect fit, while the minimum NSE value is $-\infty$; in this study an average NSE value of 0.75 was calculated for the 10 different rainfall events used in the calibration phase. The verification was also conducted on 10 different events, dedicated for verification purpose and not participating in the calibration process, and an average NSE equivalent to 0.71 was found. Using the EPA-SWMM calibrated model, the UDS was subjected to a measured severe storm event on 31 August 2015 (Abou Rjeily *et al.* 2016). In addition to the similarities between measured and simulated values, model simulation results indicate the appearance of floods at the same locations and with the same water depths as were measured during this event.

Analysis of the UDS performance

Results from the EPA-SWMM model simulation of the event on 31 August 2015 suggest a total flood volume and duration for all manholes of 869 m^3 and 40.3 hours. The results show the flooding to be from manholes with low ground elevations. The main collector being surcharged, water flows back into the secondary branches and induces floods on the campus. Simulation results show that the limitation of the hydraulic capacity is due to the static equipment installed on the UDS (check valve and flow regulator presented in Figure 2).

Due to the stochastic nature of storm events, interpreted by temporal variability of rainfall intensities, the operation of the UDS was also studied on the synthetic events of 1, 2 and 5 year return period (YRP). In this paper, the double triangular synthetic rainfall event, which provides a good representation of the actual structure of storm events at the university area (Hémain 1986), was used for the analysis of the UDS. Based on the response time of the watershed and the characteristics of the observed rainfall events within the studied area, the high intensity duration and total duration of the synthetic events were chosen to be 15 minutes and 2 hours, respectively. Characteristics of the three synthetic events are presented in Table 1. The results with a 5 YRP event confirmed the results of the simulation of the

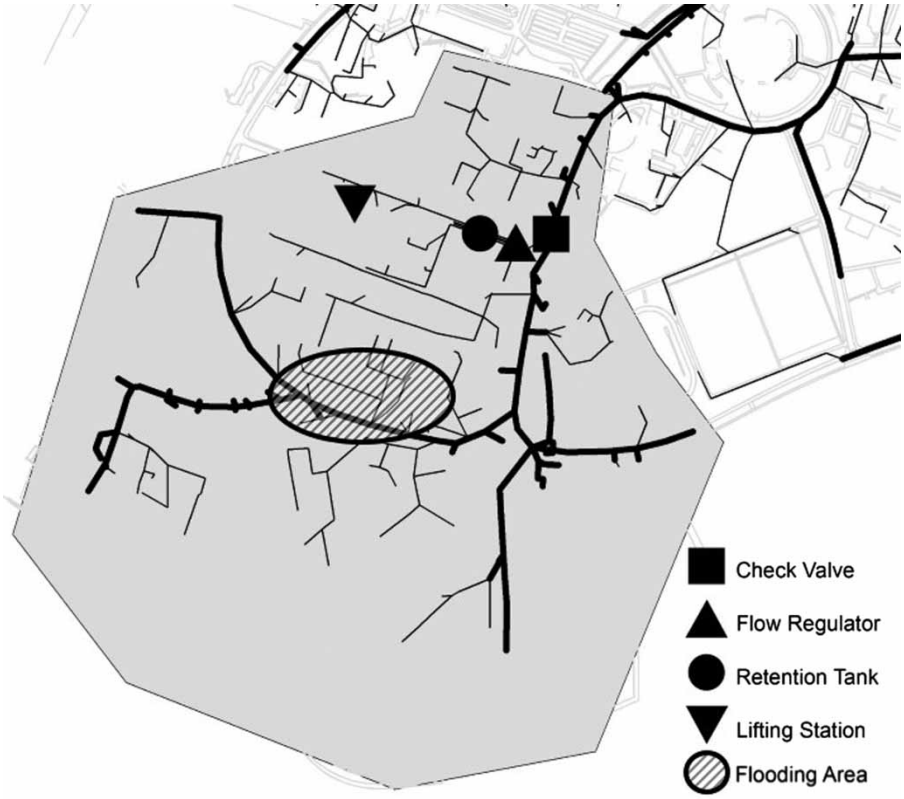

Figure 2 | Studied sector of the stormwater system with the installed equipment.

31 August 2015 storm event. The 5 YRP event generates flooding appearances in different low topographical areas due to the backflow coming from the main collector of the system, as observed in the simulation results of the 31 August 2015 event. The simulated results indicate a total flooding volume and duration for all manholes equivalent to 1,013 m^3 and 180.7 h. Minor floods were reported for the 2 YRP synthetic event, while the 1 YRP event surcharges the system without inducing floods. Based on the hydraulic model results for the 5 YRP and 31 August 2015 events, locations of the critical zones and manholes, where water depth should be monitored in order to predict flooding, were identified as presented in the next section.

Identifying the locations of the critical zones

This section presents the method used for locating the critical areas. EPA-SWMM simulation results indicate that the flooding areas are located in the lowest topographical zones, and they are due to backflow water coming from the main collector (presented in Figure 1). Critical manholes are points within the critical areas where water depth will be monitored. The critical manholes were chosen to be on the main collector, where branches of the lowest topographical areas are connected. This choice was made in order to reduce the number of critical manholes, by monitoring the water depth in the downstream manhole connecting the branch to the main collector, instead of monitoring it in each flooded manhole. In addition, monitoring the downstream manhole water depth variation helps avoid any additional complexity for the FFS, described in the following paragraphs. Backflow water responsible for the flooding in the secondary branches, generated after a certain water level in the main collector, is presented by a sudden water depth variation in the flooded manholes. By choosing to monitor the water depth variation in the downstream manholes on the main collector, the FFS is no longer required to predict these sudden variations, which results in less complexity for the system. It was also decided not to forecast water depth in two close manholes, since water depth requires a long distance to vary significantly. Therefore, a minimal distance of 120 m including at least three principal manholes was chosen to separate two successive critical manholes to monitor. Based on this criterion and the analysis of the campus UDS, five critical manholes were identified; Figure 4 shows their locations.

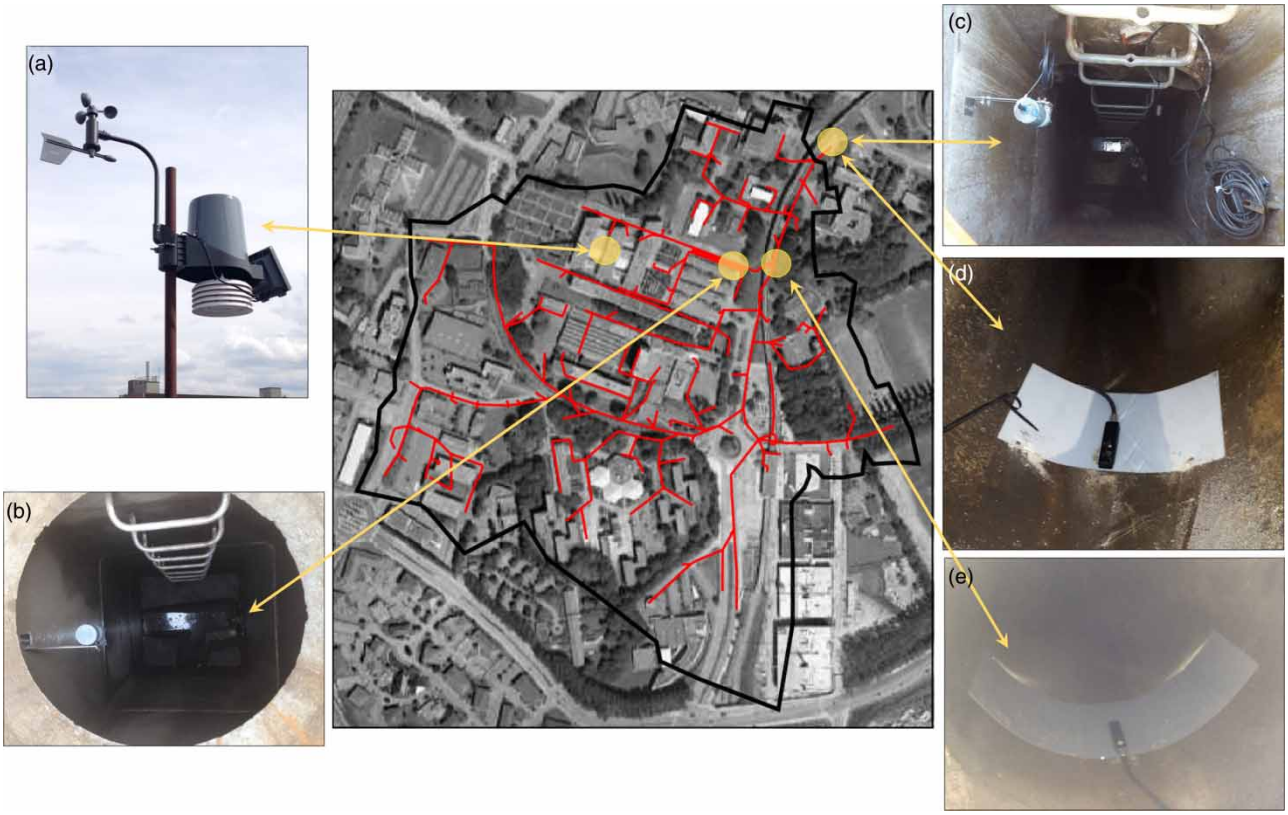

Figure 3 | The monitoring system implemented on the studied sector of Lille University campus ((a) weather station; (b) depth meter in the retention tank; (c) depth meter at the outfall; (d) flowmeter at the outfall; (e) flowmeter in the main collector).

Implementation of the FFS

The FFS is based on forecasting the water depth variation at the five critical manholes, using the predicted rainfall intensities for the entire forecasted period. The period of prediction of the FFS is limited by the capacity of the weather forecast system to predict reliable rainfall intensity values. The network architecture presents one input node for the rainfall intensity time series. Since the NARX neural network is designed to determine the water depth at five critical manholes, five nodes in the output layer are required, as shown in Figure 5. After several trials, the

Table 1 | Characteristics of the three synthetic storm events

Synthetic event return period	Total duration [min]	High intensity duration [min]	Total depth [mm]	Peak intensity [mm/hr]
1 YRP	120	15	17.37	55.3
2 YRP	120	15	22.82	68.6
5 YRP	120	15	32.35	94.5

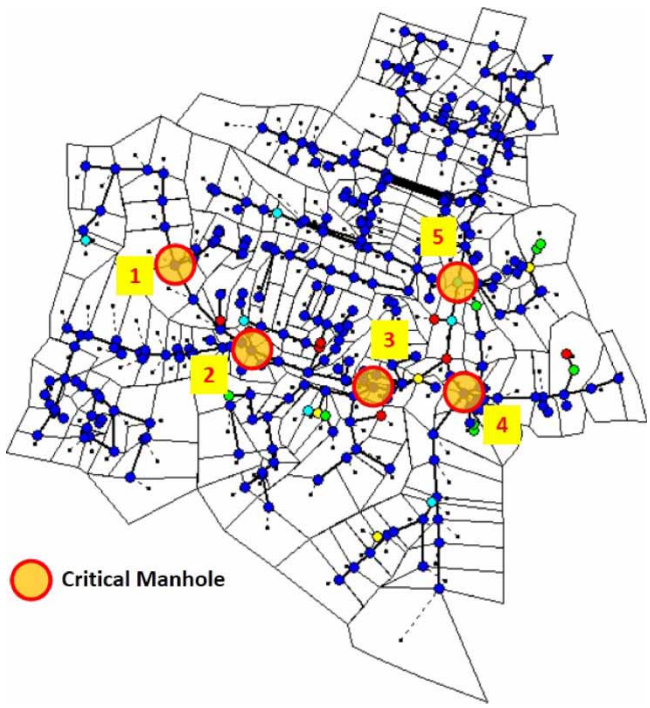

Figure 4 | Locations of the critical manholes.

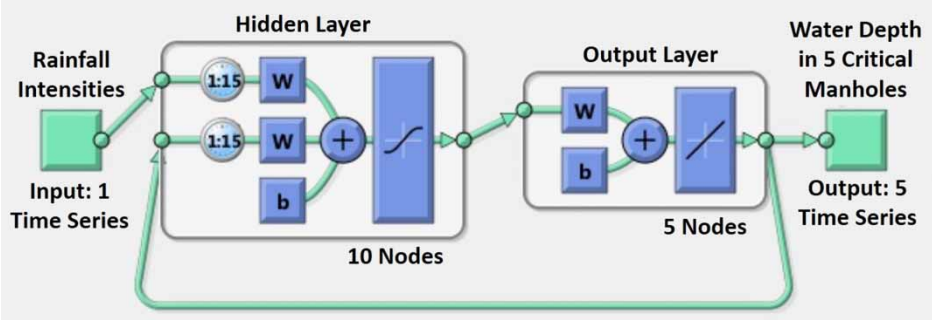

Figure 5 | NARX neural network for forecasting flooding events (W and b refer to weights and biases).

training results show that one hidden layer with 10 nodes and 15 time step delays for the exogenous input and the recurrent output signals were sufficient to enable the NARX neural network to operate well on the measured events. These results were obtained by using the hyperbolic tangent sigmoid and linear functions as transform functions for the hidden and output layers, respectively.

The FFS was trained on 10 different storm events, measured by the implemented monitoring system and presented in Table 2. Measured rainfall intensities and modelled water depth variations in the five critical manholes were introduced as input and target values for the NARX neural network training process, respectively. The Levenberg–Marquardt backpropagation training function was selected to train the FFS. The Levenberg–Marquardt function is considered as the fastest training function and has been very successfully applied for neural networks. Its efficiency is limited for large networks with thousands of weights, where it requires more memory space and computation time (Hagan *et al.* 1996; Demuth *et al.* 2008), which is not the case for the FFS to be developed in this study. The mean squared error (MSE) performance function was used for evaluating the training process through the iterations. 'mapminmax' was used as the pre- and post-processing function for input and output layers to rearrange their values within the range of [−1 1]. This 'mapminmax' function was necessary in this NARX neural network in order to avoid high weighted input values for the hyperbolic tangent sigmoid transfer function in the neurons of the hidden layer, and thus avoid the saturation of these functions, followed by a shallow gradient of reduction in MSE and hence a slow training process.

Table 2 | Rainfall events for calibration and verification purposes

Date	Total duration [min]	Total depth [mm]	Peak intensity [mm/hr]
25/07/2015	320	13.04	16.76
30/07/2015	30	5.55	59.95
04/08/2015	51	6.65	86.36
26/08/2015	46	9.77	39.62
13/09/2015	274	20.84	96.27
05/10/2015	1,026	12.03	7.87
31/08/2015	164	24.35	217.18
19/11/2015	430	17.29	22.61
11/12/2015	172	5.81	23.37
30/01/2016	452	11.33	13.97

Training results

The NARX neural network shows very good correlation and efficiency on the historical measurements data set that was randomly divided into training (70%), validation (15%) and testing (15%) sub-divisions. Figure 6 presents the

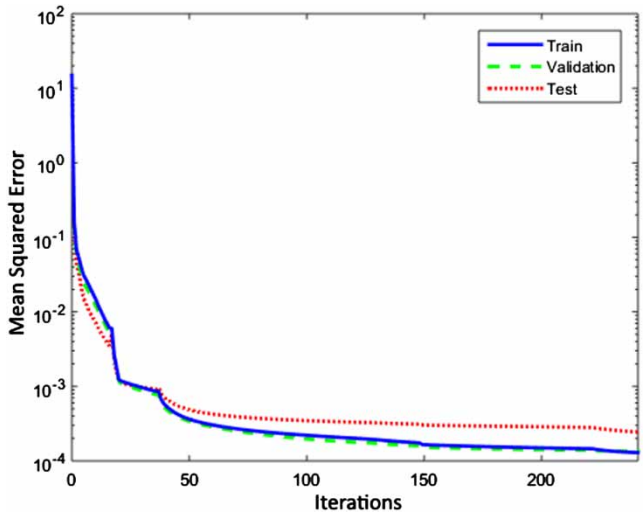

Figure 6 | Performance evaluation through the iterations of the training process.

performance improvements of the NARX neural network during the iterations of the training process. Figure 7 shows the regression results of the different sub-divisions after the training process was completed. Regression results were found by comparing the calculated outputs with the targets through data points representing water depth at each time step for all the monitored locations.

The training process reduced the MSE value from 14 to 1.3×10^{-4} in 235 iterations. The efficiency of the trained network was presented by very good regression values (R). An R equal to 0.999 is presented for the training data subdivision, while R values equivalent to 0.998 and 0.994 were found for the validation and testing parts respectively. These results highlight the efficiency of the constructed neural network during the training process and in forecasting the water depth in the five critical manholes during the 10 measured rainfall events.

Verification and discussions

After training, validating and testing the FFS using the measured rainfall events had shown good results, further validation of the system was carried out on the synthetic rainfall events with 1, 2 and 5 YRP. These synthetic events were not used in the training phase. The EPA-SWMM hydrologic-hydraulic model was used for modelling the three synthetic events. The rainfall intensities of the three synthetic events

Table 3 | NSE for the five critical manholes

Return period	Manhole 1	Manhole 2	Manhole 3	Manhole 4	Manhole 5
One year	0.39	0.86	0.95	0.82	0.94
Two years	0.87	0.90	0.85	0.85	0.82
Five years	0.93	0.95	0.95	0.92	0.89

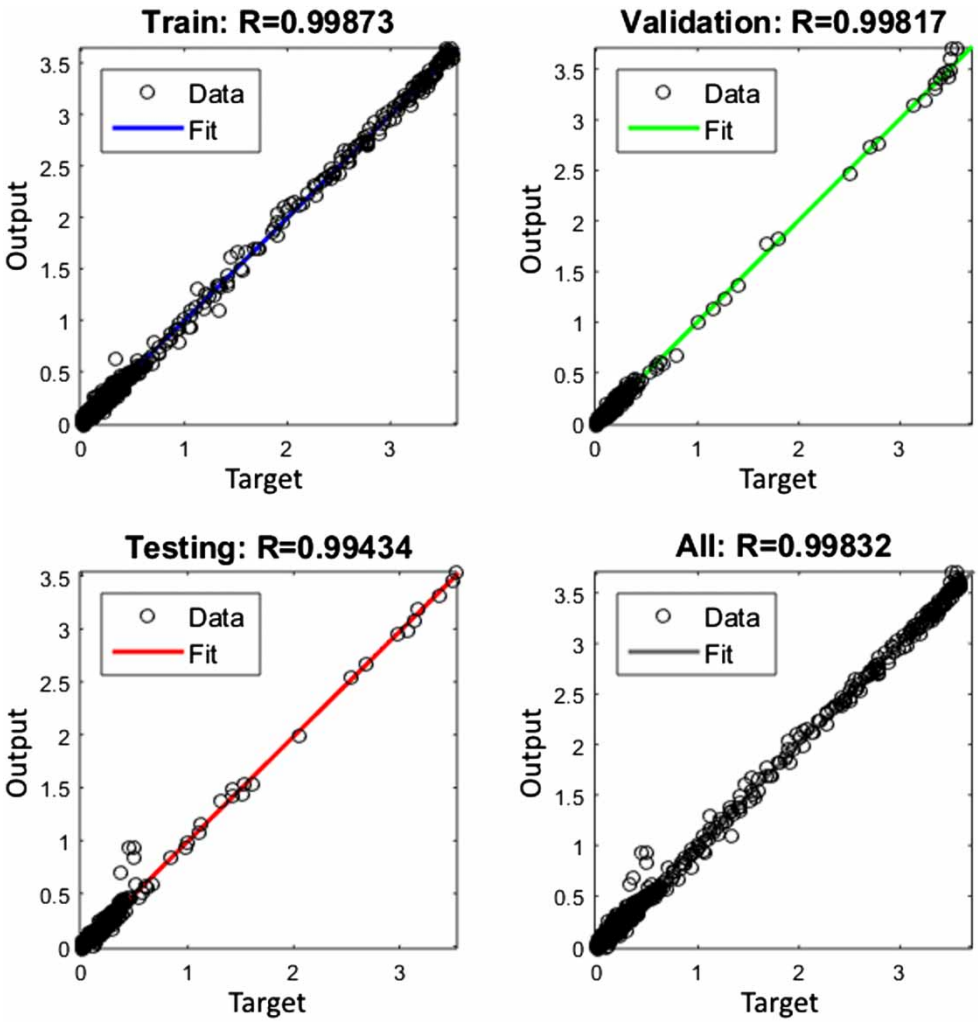

Figure 7 | Regression results of the trained NARX neural network.

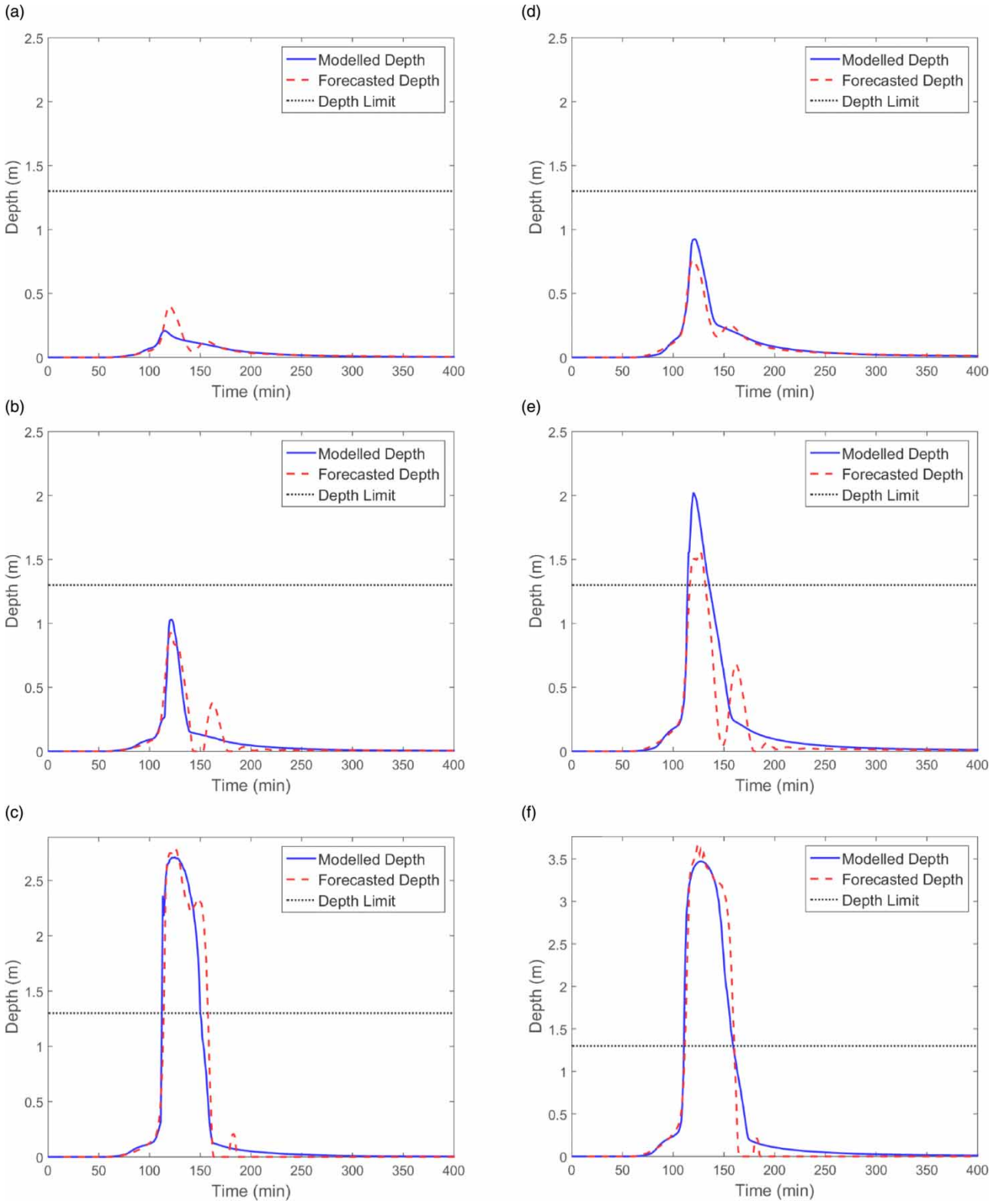

Figure 8 | Comparison between EPA-SWMM simulation results and NARX neural network outputs for the critical manholes 1 and 3 ((a) manhole 1 – 1 YRP event; (b) manhole 1 – 2 YRP event; (c) manhole 1 – 5 YRP event; (d) manhole 3 – 1 YRP event; (e) manhole 3 – 2 YRP event; (f) manhole 3 – 5 YRP event).

were introduced in the NARX neural network, in order to get the FFS forecasted results and compare them to the EPA-SWMM simulation results. The 2 and 5 YRP storm events induce floods; therefore they were used to test the system capacity in forecasting flooding events. The 1 YRP storm event was necessary for testing the system robustness in generating significant and not erroneous alarms. NSE - coefficients for the water depth variation in the five critical manholes during the three synthetic events are presented in Table 3.

Except for manhole 1 during the 1 YRP synthetic event, the calculated NSE coefficients represent relatively high values, affirming the capacity of the NARX neural network in representing the water depth variation during a rainfall event. The results show the efficiency of the developed FFS, especially for the intense storm events, as presented for the synthetic event of 5 YRP. The calculated NSE value, which is relatively low for the critical manhole 1 under the 1 YRP, was graphically analysed and it was found to be due to the small water depth values reached in this manhole during this event. Therefore, this observation does not indicate a limitation of the FFS that aims to detect flooding, which appears on high water depth values in the critical manholes. Figure 8(a) presents the water depth variation for manhole 1 during the 1 YRP synthetic event.

Considering the importance of the peak water depth, Table 4 presents the modelled over the forecasted peak values for the five critical manholes.

Similarly, the results of the modelled over forecasted peak ratio are considered as a very good indicator of the FFS efficiency in alerting the UDS managers of high risk events. The results of the synthetic event of 2 YRP were used to define the water level limit, where the floods began to appear in the adjacent areas of the monitored critical manholes. During this event, water levels in the flooding areas reach the limit of the total depth of the manholes, with some minor flooding, not exceeding a 1 cm depth. By inspecting the water depth in the defined critical manholes during this event, it was found that a water level limit equivalent to 1.3 m is efficient for detecting flooding occurrences in the neighbourhood areas of the critical manholes. Figure 8 presents the modelled and forecasted water depth variations for two of the five critical manholes (manhole 1 and 3), during the three synthetic events.

These figures show good correlations between the simulated and the FFS forecasted results. By comparing the manhole water depth with the water depth threshold, it is clear that an alarm will be activated for the storm event of 5 YRP, indicating flood risk in all the branches connected to the five critical manholes. For the event of 2 YRP, results show that an alarm will be activated for all manholes except the critical manhole 1. This result was examined on the EPA-SWMM model, and no floods were mentioned in the branches connected to this manhole during the 2 YRP event. No alarms had been activated for the synthetic event of 1 YRP, which is a good observation, indicating the capacity of the system in generating representative and not erroneous alarms. It is better to define the threshold level to trigger alarms slightly below 1.3 m in order to maintain a security factor. The results of the modelled over forecasted peaks, presented in Table 4, could assist in defining the optimal security factor.

Table 4 | Modelled over forecasted peak values for the five critical manholes

Return period	Manhole 1	Manhole 2	Manhole 3	Manhole 4	Manhole 5
One year	0.52	0.78	1.22	1.49	1.00
Two years	1.11	1.25	1.30	1.31	0.93
Five years	0.97	0.96	0.95	0.91	0.87

CONCLUSION

This paper presented the development and the use of an FFS. A fast and efficient tool, based on the NARX neural network, was developed to rapidly alert UDS managers of flood risks. The choice of NARX neural network was based on its calculation nature, in combining multiple precedent inputs with outputs calculated in previous time steps in the prediction of the output for the next time step. This nature showed a high efficiency of the developed FFS in representing the real UDS response to a forecasted storm event. The application of the FFS on the UDS of the campus of the University of Lille shows that the trained NARX neural network performed well on both minor and severe storm events. It constitutes a robust and efficient tool for flooding forecast that could be simply applied to any other networks. The advantage offered by the NARX neural network over a regular simulation model is its calculation speed. Instead of simulating the entire system operation with complex hydrologic–hydraulic phenomena, which requires computation time according to the model size and rainfall duration, the FFS proposed in this work delivers the results in less than 1 second, through simple and fast arithmetic calculations. Since the FFS developed in this work is based on a weather forecast system, the accuracy of the forecasted rainfall intensities plays an important role in the efficiency of the FFS. Weather forecasting systems lose

their prediction accuracy with longer forecasting periods. Therefore, users are encouraged to periodically re-start the fast FFS calculation with each weather forecast update.

REFERENCES

Abou Rjeily, Y., Sadek, M., Shahrour, I. & Hage Chehade, F. 2016 Dynamic management through inline monitoring of stormwater systems. In: *8th International Conference on Sewer Processes and Networks*, IWA, Rotterdam.

Amarnath, G., Alahacoon, N., Gismalla, Y., Mohammed, Y., Sharma, B. R. & Smakhtin, V. 2016 Increasing early warning lead time through improved transboundary flood forecasting in the gash river Basin, Horn of Africa. In: *Flood Forecasting* (T. E. Adams & T. C. Pagano, eds). Academic Press, Boston, pp. 183–200.

Artinyan, E., Vincendon, B., Kroumova, K., Nedkov, N., Tsarev, P., Balabanova, S. & Koshinchanov, G. 2016 Flood forecasting and alert system for Arda River basin. *Journal of Hydrology* **541**, 457–470.

Asgari, H., Chen, X., Morini, M., Pinelli, M., Sainudiin, R., Spina, P. R. & Venturini, M. 2016 NARX models for simulation of the start-up operation of a single-shaft gas turbine. *Applied Thermal Engineering* **93**, 368–376.

Beeneken, T., Erbe, V., Messmer, A., Reder, C., Rohlfing, R., Scheer, M., Schuetze, M., Schumacher, B., Weilandt, M. & Weyand, M. 2013 Real time control (RTC) of urban drainage systems – a discussion of the additional efforts compared to conventionally operated systems. *Urban Water Journal* **10** (5), 293–299.

Berggren, K., Olofsson, M., Viklander, M., Svensson, G. & Gustafsson, A.-M. 2012 Hydraulic impacts on urban drainage systems due to changes in rainfall caused by climatic change. *Journal of Hydrologic Engineering* **17** (1), 92–98.

Brandes, D., Cavallo, G. J. & Nilson, M. L. 2005 Base flow trend in urbanizing watersheds of the Delaware River basin. *JAWRA Journal of the American Water Resources Association* **41** (6), 1377–1391.

Çoruh, S., Geyikçi, F., Kılıç, E. & Çoruh, U. 2014 The use of NARX neural network for modeling of adsorption of zinc ions using activated almond shell as a potential biosorbent. *Bioresource Technology* **151**, 406–410.

Demuth, H., Beale, M. & Hagan, M. 2008 *Neural Network Toolbox™ 6. User's Guide*. MathWorks, Inc., Natick, MA, USA.

Duncan, A., Chen, A. S., Keedwell, E., Djordjevic, S. & Savic, D. 2013 RAPIDS: early warning system for urban flooding and water quality hazards. In: *Machine Learning in Water Systems Symposium: Part of AISB Annual Conference*, pp. 1–5.

Elsafi, S. H. 2014 Artificial neural networks (ANNs) for flood forecasting at Dongola Station in the River Nile, Sudan. *Alexandria Engineering Journal* **53** (3), 655–662.

García, L., Barreiro-Gomez, J., Escobar, E., Téllez, D., Quijano, N. & Ocampo-Martinez, C. 2015 Modeling and real-time control of urban drainage systems: a review. *Advances in Water Resources* **85**, 120–132.

Hagan, M. T., Demuth, H. B. & Beale, M. 1996 *Neural Network Design*. PWS Publishing Co., Boston.

Hémain, J.-C. 1986 *Modélisation de l'écoulement dans les réseaux: guide de construction et d'utilisation des pluies de projet*. Service Technique de l'Urbanisme, Division des équipements urbains, Paris.

Hoffmeister, F. 1991 Scalable parallelism by evolutionary algorithms. In: *Parallel Computing and Mathematical Optimization: Proceedings of the Workshop on Parallel Algorithms and Transputers for Optimization* (M. Grauer & D. B. Pressmar, eds). Springer, Berlin, pp. 177–198.

Kenyon, W., Hill, G. & Shannon, P. 2008 Scoping the role of agriculture in sustainable flood management. *Land Use Policy* **25** (3), 351–360.

Konrad, C. P. & Booth, D. B. 2002 *Hydrologic Trends Associated with Urban Development for Selected Streams in the Puget Sound Basin, Western Washington*. US Department of the Interior, US Geological Survey, Tacoma, Washington, USA.

Marsalek, J. 2000 Overview of flood issues in contemporary water management. In: *Flood Issues in Contemporary Water Management* (J. Marsalek, W. E. Watt, E. Zeman & F. Sieker, eds). Springer, Dordrecht, pp. 1–16.

May, W. 2008 Potential future changes in the characteristics of daily precipitation in Europe simulated by the HIRHAM regional climate model. *Climate Dynamics* **30** (6), 581–603.

Menezes Jr., J. M. P. & Barreto, G. A. 2008 Long-term time series prediction with the NARX network: an empirical evaluation. *Neurocomputing* **71** (16–18), 3335–3343.

Nash, J. E. & Sutcliffe, J. V. 1970 River flow forecasting through conceptual models part I – a discussion of principles. *Journal of Hydrology* **10** (3), 282–290.

Ocampo-Martinez, C. 2010 *Model Predictive Control of Wastewater Systems*. Springer Science & Business Media, London.

Perera, E. D. P. & Lahat, L. 2015 Fuzzy logic based flood forecasting model for the Kelantan River basin, Malaysia. *Journal of Hydro-Environment Research* **9** (4), 542–553.

Ponce, V. M., Lohani, A. K. & Huston, P. T. 1997 Surface albedo and water resources: hydroclimatological impact of human activities. *Journal of Hydrologic Engineering* **2** (4), 197–203.

Rajendra Acharya, U., Subbanna Bhat, P., Iyengar, S. S., Rao, A. & Dua, S. 2003 Classification of heart rate data using artificial neural network and fuzzy equivalence relation. *Pattern Recognition* **36** (1), 61–68.

Rocha, H., Dias, J. M., Ferreira, B. C. & do Carmo Lopes, M. 2013 On the use of a priori knowledge in pattern search methods: application to beam angle optimization for intensity-modulated radiation therapy. In: *Computational Science and its Applications – ICCSA 2013: 13th International Conference, Ho Chi Minh City, Vietnam, June 24–27, 2013, Proceedings, Part I* (B. Murgante, S. Misra, M. Carlini, C. M. Torre, H.-Q. Nguyen, D. Taniar, B. O. Apduhan & O. Gervasi, eds). Springer, Berlin, pp. 279–292.

Tijani, I. B., Akmeliawati, R., Legowo, A. & Budiyono, A. 2014 Nonlinear identification of a small scale unmanned helicopter using optimized NARX network with

multiobjective differential evolution. *Engineering Applications of Artificial Intelligence* **33**, 99–115.

Wang, L., Lyons, J. & Kanehl, P. 2003 Impacts of urban land cover on trout streams in Wisconsin and Minnesota. *Transactions of the American Fisheries Society* **132** (5), 825–839.

Yen-Ming, C., Li-Chiu, C., Meng-Jung, T., Yi-Fung, W. & Fi-John, C. 2010 Dynamic neural networks for real-time water level predictions of sewerage systems-covering gauged and ungauged sites. *Hydrology and Earth System Sciences* **14** (7), 1309–1319.

First received 14 February 2017; accepted in revised form 27 June 2017. Available online 10 July 2017